

EPISTASIS AND SHAPES OF FITNESS LANDSCAPES

Niko Beerenwinkel, Lior Pachter, and Bernd Sturmfels

Department of Mathematics, University of California at Berkeley

Abstract: The relationship between the shape of a fitness landscape and the underlying gene interactions, or epistasis, has been extensively studied in the two-locus case. Gene interactions among multiple loci are usually reduced to two-way interactions. We present a geometric theory of shapes of fitness landscapes for multiple loci. A central concept is the genotope, which is the convex hull of all possible allele frequencies in populations. Triangulations of the genotope correspond to different shapes of fitness landscapes and reveal all the gene interactions. The theory is applied to fitness data from HIV and *Drosophila melanogaster*. In both cases, our findings refine earlier analyses and reveal previously undetected gene interactions.

Key words and phrases: Convex polytope, Epistasis, fitness landscape, gene interaction, genotope space, human genotope, population simplex, triangulation

1. Introduction

The term “epistasis” was coined by Bateson (1909) to describe the interactions among individual genes. The concept was introduced in the setting of Mendelian genetics, where epistasis gives rise to distorted Mendelian ratios of genotypes. In the context of statistical genetics, epistasis was originally called “epistacy” by Fisher (1918). Here, it arises when mapping discrete genotypes to continuous traits and refers to contributions to the phenotype that are not linear in the average effects of the single genes. The phenotypic trait of an organism that drives the evolution of the population is the reproductive fitness of individuals, i.e., the expected number of offspring. For this trait, the genotype–phenotype mapping is called a fitness landscape (Gavrilets, 2004; Wright, 1931), and epistasis is a property of that landscape.

For a genetic system of two biallelic loci, there is only one type of interaction, illustrated by the landscapes in Figure 1.1, and epistasis refers unambiguously to this interaction. However, the situation is more complex for more than two loci, because new interaction patterns arise. The current language for describing

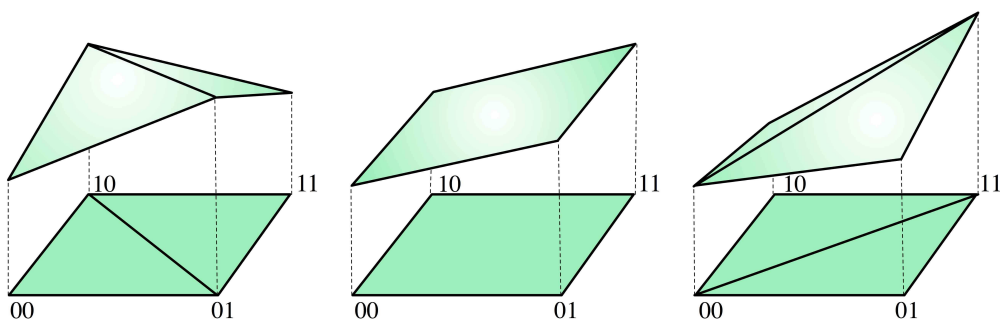


Figure 1.1: The possible shapes of fitness landscapes on two biallelic loci. The genotype is the square. Its two triangulations correspond to negative and positive epistasis.

gene interactions does not reflect this diversity (Phillips, 1998). Indeed, the common approach of investigating epistasis by analysis of variance (ANOVA) and expressing epistatic effects as the residuals of a linear regression of fitness on the genotypes (Cordell, 2002) does not account for the intrinsic combinatorial structure of the landscapes that generalize two-locus epistasis.

For a specified set of genotypes that may involve multiple loci, we characterize all possible interactions among them. Our characterization is based on a geometric object, the *genotope*, which is the convex hull of the possible allele frequency vectors. The regular triangulations (De Loera et al., 2006) of the genotope encode the genotype interactions in the fitness landscape. The biological problem of studying genotype interactions for a fitness landscape is thus equivalent to the combinatorial problem of finding the shape of the fitness landscape, i.e., the triangulation of the genotope that is induced by the fitness landscape.

In Sections 2 to 4, the mathematical concepts are introduced and illustrated in several examples. For simplicity, we focus primarily on the case of a population of haploid individuals (or, equivalently, of homozygous diploids). Nevertheless, our concepts and algorithms are not limited to haploids, and in Example 2.5 we briefly indicate the modifications necessary for diploids.

In Section 5, we discuss the three-locus two-allele system, which amounts to classifying the 74 triangulations of the 3-cube. Table 5.1 is the direct generalization of the list of possible shapes for two biallelic loci, shown in Figure 1.1.

In Sections 6 and 7, we apply our method to two published fitness land-

scapes. Section 6 deals with a biallelic three-locus system in HIV (Segal et al., 2004) and emphasizes the modeling of measurement error. Section 7 revisits the five-locus system in *Drosophila melanogaster* studied by Whitlock and Bourguet (2000). The shape of their *Drosophila* fitness landscape is a triangulation of the 5-dimensional cube (the genotope) into 110 simplices, listed in Figure 7.7.

Our discussion in Section 8 compares our approach with other studies of fitness landscapes. It also raises the challenge of determining the *human genotope* and its biologically relevant triangulations from suitable haplotype data.

2. Populations and the Genotope

We fix a finite alphabet Σ of size l , which labels the l different alleles at a genetic locus of interest. The elements of Σ may correspond to variants of a gene, to the nucleotides at a genome position ($\Sigma = \{\text{A, C, G, T}\}$, $l = 4$), or to the amino acids at a codon position in a gene ($l = 20$). The biallelic case ($\Sigma = \{0, 1\}$, $l = 2$) arises frequently in genomics, where it is known that most SNPs (single nucleotide polymorphisms) have two types.

The allele frequencies at a certain locus define a probability distribution on the alphabet Σ . The set of all probability distributions on Σ is identified with the $(l - 1)$ -dimensional standard simplex

$$\Delta_{\Sigma} = \{(p_1, p_2, \dots, p_l) \in [0, 1]^l : p_1 + p_2 + \dots + p_l = 1\}.$$

We consider n loci, all with the same alphabet Σ of alleles, and we denote by Σ^n the set of sequences of length n over Σ . The elements of Σ^n are identified with the vertices of the n -fold direct product of simplices $\Delta_{\Sigma}^n = (\Delta_{\Sigma})^n$. This product is a convex polytope (Ziegler, 1995) of dimension $ln - n$ having l^n vertices. In particular, in the binary case, $\Delta_{\{0,1\}}^n$ is the standard n -dimensional cube.

A *genotype space* is any subset \mathcal{G} of Σ^n . For a given genotype space \mathcal{G} , let $\Pi_{\mathcal{G}}$ be the convex hull of all vertices in Δ_{Σ}^n that are indexed by sequences in \mathcal{G} . The set $\Pi_{\mathcal{G}}$ is a subpolytope of Δ_{Σ}^n . We call $\Pi_{\mathcal{G}}$ the *genotope*. A point v in the genotope is an n -tuple of allele frequencies. To be precise, if $v = (v_1, \dots, v_n) \in \Pi_{\mathcal{G}} \subseteq \Delta_{\Sigma}^n$ then $v_i \in \Delta_{\Sigma}$ represents the allele frequencies at locus i .

Example 2.1. (Genotype lattices)

In the study of directed evolution in (Beerenwinkel et al., 2006) the alphabet is

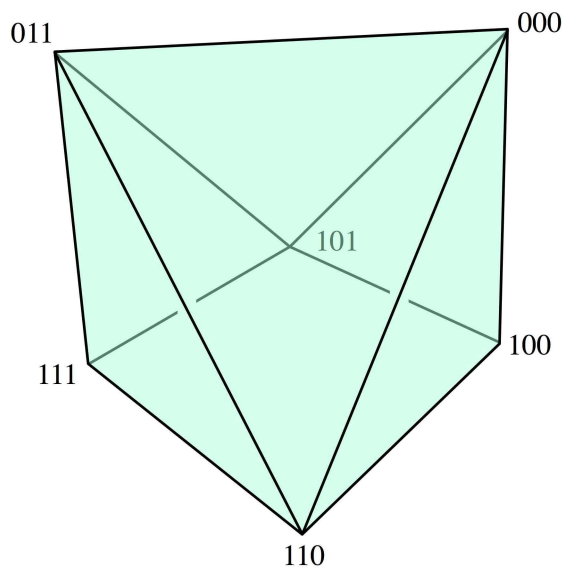


Figure 2.2: A three-dimensional genotype from the HIV data of Section 6.

$\Sigma = \{0, 1\}$ and the genotype space \mathcal{G} is the distributive lattice induced by an event poset \mathcal{E} with n elements. The genotype $\Pi_{\mathcal{G}}$ is the *order polytope* of the poset \mathcal{E} . If the event poset \mathcal{E} is empty then $\mathcal{G} = \{0, 1\}^n$, the genotype $\Pi_{\mathcal{G}}$ is the n -dimensional cube. The case $n = 2$ is Example 2.4. The case $n = 3$ is discussed in detail in Section 4. For an example of a non-empty event poset consider $n = 3$ and $\mathcal{E} = \{2 < 3\}$, meaning that the second event has to occur before the third event can happen. The induced genotype lattice has six genotypes,

$$\mathcal{G} = \{000, 001, 011, 100, 101, 111\}, \quad (2.1)$$

and the corresponding genotype $\Pi_{\mathcal{G}}$ is a triangular prism. \square

Example 2.2. (A genotype from HIV fitness data)

Consider the genotype space

$$\mathcal{G} = \{000, 110, 011, 100, 101, 111\}, \quad (2.2)$$

which differs from the one in (2.1) only by the second genotype. This \mathcal{G} does not form a distributive lattice, so it does not arise in the setting of (Beerenwinkel et

al., 2006). The genotype $\Pi_{\mathcal{G}}$ has six triangular faces and one square face (Figure 2.2). This genotype appears in our analysis of the HIV data in Section 6. \square

By a *population* on \mathcal{G} we shall mean any probability distribution p on the set \mathcal{G} . For any genotype $g \in \mathcal{G}$, the coordinate p_g of p represents the fraction of the population that is of genotype g . A population is a point in the *population simplex* $\Delta_{\mathcal{G}}$. The population simplex and the genotype are related via the marginalization map ρ , which maps a population p to its n -tuple of allele frequencies,

$$\rho : \Delta_{\mathcal{G}} \rightarrow \Pi_{\mathcal{G}} \subset \Delta_{\Sigma}^n, \quad (p_{\sigma_1 \dots \sigma_n})_{\sigma \in \Sigma^n} \mapsto \left(\left(\sum_{\sigma: \sigma_i = \tau} p_{\sigma_1 \dots \sigma_n} \right)_{\tau \in \Sigma} \right)_{i=1, \dots, n}.$$

If the population p consists of a single genotype g , then p is the unit vector whose coordinates are $p_g = 1$ and $p_h = 0$ for all $h \in \mathcal{G} \setminus \{g\}$. Its allele frequency vector $\rho(g)$ is a list of n unit vectors, each of length l . The unit vector $\rho(g)_i$ is the vertex of the simplex Δ_{Σ} indexed by the i -th allele of the genotype g . Thus $\rho(g)$ is a vertex of the genotype $\Pi_{\mathcal{G}}$, and all vertices arise in this manner. Since the marginalization map ρ is linear, we conclude:

Proposition 2.3. *The genotype $\Pi_{\mathcal{G}}$ equals the set of all possible n -tuples of allele frequencies that may arise from a population on the genotype space \mathcal{G} .*

Example 2.4. (Tetrahedron maps onto square)

Let $n = 2$, $\Sigma = \{0, 1\}$, and consider the genotype space $\mathcal{G} = \{00, 01, 10, 11\}$. The set $\Delta_{\mathcal{G}}$ of probability distributions on \mathcal{G} is a tetrahedron in 4-space,

$$\Delta_{\mathcal{G}} = \{(p_{00}, p_{01}, p_{10}, p_{11}) \in [0, 1]^4 \mid p_{00} + p_{01} + p_{10} + p_{11} = 1\}.$$

The genotype $\Pi_{\mathcal{G}}$ is the square $\Delta_{\Sigma} \times \Delta_{\Sigma}$. A population p is a point in the tetrahedron whose allele frequencies are given by the marginalization map

$$\rho(p_{00}, p_{01}, p_{10}, p_{11}) = ((p_{00} + p_{01}, p_{10} + p_{11}), (p_{00} + p_{10}, p_{01} + p_{11})).$$

If we identify the square $\Pi_{\mathcal{G}} = \Delta_{\Sigma}^2$ with the convex hull of the four points $(0, 0)$, $(0, 1)$, $(1, 0)$, $(1, 1)$ in the plane, then the marginalization map is the following projection (see Figure 2.3) from the tetrahedron onto the square:

$$\rho(p_{00}, p_{01}, p_{10}, p_{11}) = (p_{10} + p_{11}, p_{01} + p_{11}).$$

The two coordinates are the frequencies at the two loci of the allele “1”. \square

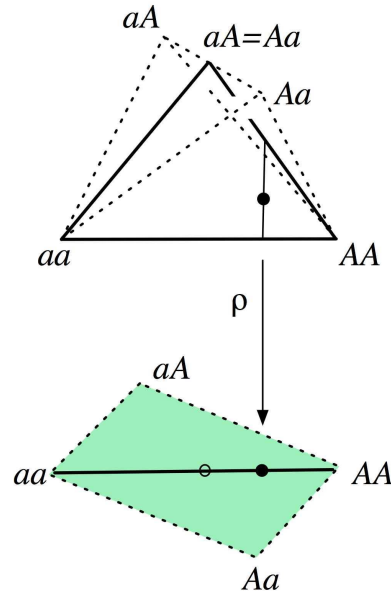


Figure 2.3: Population simplex and genotype for one diploid biallelic locus.

Example 2.5. (From haploids to diploids)

The mathematical set-up introduced so far is for haploids only. It can be extended to diploids using either of the following two equivalent approaches. The allele frequencies of diploid populations can be modeled by scaling each simplex in Δ_{Σ}^n by a factor of two, so that the genotype sits inside $(2\Delta_{\Sigma})^n$. Alternatively, we could replace n by $2n$ and then restrict to symmetric populations in Δ_{Σ}^{2n} .

To illustrate both approaches, we consider a single biallelic locus ($l = 2$, $n = 1$) with genotypes aa, AA, aA, Aa , where we identify Aa with aA . The population simplex is a triangle, and the genotype $2\Delta_{\Sigma}$ is a line segment whose end points are labeled aa and AA and whose midpoint is labeled by $Aa = aA$. This picture arises from $\Delta_{\Sigma^2} \rightarrow \Delta_{\Sigma}^2$ by intersecting with a plane. The genotype is the diagonal segment in the square of Example 2.4, and the population triangle is a cross-section of the tetrahedron, depicted in Figure 2.3. A point in the population triangle has three coordinates (p_{aa}, p_{aA}, p_{AA}) where p_{aa} is the frequency of genotype aa , p_{AA} that of genotype AA , and $2p_{aA}$ that of genotype $Aa = aA$. \square

Returning to the general haploid model, we give an interpretation of the

fiber of a point in the genotope $\Pi_{\mathcal{G}}$ under the marginalization map ρ . The fiber over $v \in \Pi_{\mathcal{G}}$ is the following polytope inside the population simplex:

$$\rho^{-1}(v) = \{ p \in \Delta_{\mathcal{G}} : \rho(p) = v \}. \quad (2.3)$$

Remark 2.6. *If v is any n -tuple of allele frequencies then its fiber $\rho^{-1}(v)$ consists of all populations p which have the specified allele frequencies v .*

If all coordinates of v are non-zero, then $\rho^{-1}(v)$ is a polytope of dimension

$$c(\mathcal{G}) = \dim(\Delta_{\mathcal{G}}) - \dim(\Pi_{\mathcal{G}}) = |\mathcal{G}| - \dim(\Pi_{\mathcal{G}}) - 1. \quad (2.4)$$

For the full genotype space $\mathcal{G} = \Sigma^n$ we have $c(\mathcal{G}) = l^n - n - 1$. In particular, in Example 2.4 the dimension is one, and in Example 2.2 the dimension is two.

Since the fibers (2.3) over the genotope $\Pi_{\mathcal{G}}$ characterize populations with constant allele frequency vectors, we can restrict our attention to these fibers whenever the allele frequencies are fixed. For example, if evolution acts on the genotype space by recombination, but without mutation and selection, then the allele frequencies of the population are constant for every generation. Hence, such evolutionary dynamics can be modeled by a dynamical system on $\rho^{-1}(v)$.

Our geometric theory is adapted to the fact that, in biological systems, the set \mathcal{G} of observed genotypes is usually significantly smaller than the number l^n of possible genotypes. Specifically, for binary data ($l = 2$) on many loci (say, $n \geq 20$), the genotope is never an n -cube, and its dimension is smaller than n due phenomena such as linkage. The frequently heard assertion that dimensions of genotype spaces and fitness landscapes increase exponentially in the sequence length is thus misleading. Even for large data sets, the complexity of the genotope $\Pi_{\mathcal{G}}$ can be expected to be in the tractable range of polyhedral algorithms.

3. Fitness Landscapes and Interaction Coordinates

A *fitness landscape* on a genotype space \mathcal{G} is a function $w: \mathcal{G} \rightarrow \mathbb{R}$. Each coordinate w_g of w denotes the logarithm of the reproductive fitness of genotype g . The space of all fitness landscapes is the $|\mathcal{G}|$ -dimensional \mathbb{R} -vector space $\mathbb{R}^{\mathcal{G}}$.

In the study of gene interactions one considers linear combinations of the measured coordinates w_g . These linear combinations express epistatic effects. Certain collections of such linear forms play the role of interaction coordinates

on $\mathbb{R}^{\mathcal{G}}$. Both the sign and the magnitude of these interaction coordinates are of interest when examining the fitness landscape w of a biological system.

Example 3.7. (Two triangles over a square)

As in Example 2.4, let $\mathcal{G} = \{0, 1\}^2 = \{00, 01, 10, 11\}$, so the genotope $\Pi_{\mathcal{G}}$ is a square. A fitness landscape w is specified by the four numbers w_{00} , w_{01} , w_{10} , and w_{11} , which we visualize as heights over the vertices of the square $\Pi_{\mathcal{G}}$. The interaction between the two loci is measured by the *epistasis*

$$u = w_{00} + w_{11} - w_{01} - w_{10}.$$

This defines three equivalence classes in the space of fitness landscapes according to whether the epistasis u is positive, negative, or zero. This trichotomy is depicted in Figure 1.1. This geometric view of genotype interaction leads us (in Section 4) to a natural concept of shapes of fitness landscapes for $n > 2$ loci. \square

Let $\mathcal{L}_{\mathcal{G}}$ be the subspace of $\mathbb{R}^{\mathcal{G}}$ consisting of all fitness landscapes w which have no interaction. Mathematically, w is in $\mathcal{L}_{\mathcal{G}}$ if there is an affine-linear function on the genotope $\Pi_{\mathcal{G}}$ whose values at the vertices are the w_g . We define the *interaction space* $\mathcal{I}_{\mathcal{G}}$ as the vector space dual to the quotient of $\mathbb{R}^{\mathcal{G}}$ modulo $\mathcal{L}_{\mathcal{G}}$:

$$\mathcal{I}_{\mathcal{G}} := (\mathbb{R}^{\mathcal{G}}/\mathcal{L}_{\mathcal{G}})^*.$$

An element of the interaction space $\mathcal{I}_{\mathcal{G}}$ is a linear form in the unknowns w_g which vanishes identically on the subspace $\mathcal{L}_{\mathcal{G}}$. In Example 2.4, the space $\mathbb{R}^{\mathcal{G}}$ is four-dimensional, its subspace $\mathcal{L}_{\mathcal{G}}$ is three-dimensional, and $\mathcal{I}_{\mathcal{G}}$ is the one-dimensional space spanned by $u = w_{00} + w_{11} - w_{01} - w_{10}$. In general, the dimension of the interaction space $\mathcal{I}_{\mathcal{G}}$ is the quantity $c(\mathcal{G})$ defined in Equation 2.4.

The interaction space $\mathcal{I}_{\mathcal{G}}$ is spanned (redundantly) by a canonical set of linear forms which are known as the *circuits*. These are the linear forms whose support (i.e., the w_g which appear with non-zero coefficient) is non-empty but minimal with respect to inclusion. The circuits in $\mathcal{I}_{\mathcal{G}}$ are unique up to scaling. Their number is usually larger than $c(\mathcal{G})$ but it is bounded above by $\binom{|\mathcal{G}|}{c(\mathcal{G})-1}$.

To see this upper bound, we note that $\mathcal{L}_{\mathcal{G}}$ has dimension $|\mathcal{G}| - c(\mathcal{G})$. The circuits of $\mathcal{I}_{\mathcal{G}}$ are computed by considering any set of $|\mathcal{G}| - c(\mathcal{G}) + 1$ of the unknowns w_g . There exists a linear combination of these w_g which vanishes on

$\mathcal{L}_{\mathcal{G}}$. If this linear combination is unique (up to scaling) then it is a circuit. The converse holds as well: all circuits in $\mathcal{I}_{\mathcal{G}}$ are found in this manner.

Example 3.8. Let \mathcal{G} be the genotype space in Example 2.2 and Figure 2.2. We have $|\mathcal{G}| = 6$ and $c(\mathcal{G}) = 2$, so our bounds say that the number of circuits is between two and six. In fact, this example has precisely four circuits:

$$\begin{aligned} f &= w_{100} - w_{101} - w_{110} + w_{111}, \\ g &= w_{000} - w_{011} - w_{100} + w_{111}, \\ n &= w_{011} + w_{101} + w_{110} - w_{000} - 2w_{111}, \\ s &= w_{000} + w_{101} + w_{110} - w_{011} - 2w_{100}. \end{aligned}$$

The names f , g , n , and s were chosen to be consistent with the discussion of the ambient 3-cube in Example 3.9. The signs of these four circuits characterize the possible interactions in any fitness landscape on the genotype space \mathcal{G} . Only eight of the 16 possible sign patterns can occur, since the linear forms f , g , n , and s lie in the two-dimensional space $\mathcal{I}_{\mathcal{G}}$. See also Figure 6.6. \square

For certain genotype spaces \mathcal{G} , the interaction space $\mathcal{I}_{\mathcal{G}}$ will have a distinguished basis consisting of *interaction coordinates*. The choice of interaction coordinates depends on the genotype $\Pi_{\mathcal{G}}$ and on the situation of interest. A natural choice exists in the case of the n -cube, where $l = 2$ and $\mathcal{G} = \{0, 1\}^n$. Consider any binary string $i_1 i_2 \cdots i_n$ which has at least two entries that are 1. For such a string $i_1 i_2 \cdots i_n$ we introduce the following element of $\mathcal{I}_{\mathcal{G}}$:

$$u_{i_1 i_2 \cdots i_n} := \frac{1}{2^{n-1}} \cdot \sum_{j_1=0}^1 \sum_{j_2=0}^1 \cdots \sum_{j_n=0}^1 (-1)^{i_1 j_1 + i_2 j_2 + \cdots + i_n j_n} \cdot w_{j_1 j_2 \cdots j_n}.$$

The number of these linear forms equals $c(\mathcal{G}) = 2^n - n - 1$, and they form a basis of $\mathcal{I}_{\mathcal{G}}$. We call the $u_{i_1 i_2 \cdots i_n}$ the interaction coordinates for the n -cube.

The linear transformation above is the *Fourier transform* for the group $(\mathbb{Z}_2)^n$. It has appeared frequently in the mathematical biology literature. For instance, Feldman et al. (1974) and Karlin and Feldman (1970) used it to study equilibria of dynamical evolutionary systems on two and three binary loci. It appears in linkage analysis (Hallgrímsson, 2005), and in phylogenetics, where it gives rise to Hadamard conjugation (Hendy and Charleston, 1993).

Example 3.9. (The 3-cube) We discuss the interaction space for the three-dimensional cube ($n = 3, l = 2$). The four interaction coordinates are

$$\begin{aligned} u_{110} &= (w_{000} + w_{001}) + (w_{110} + w_{111}) - (w_{010} + w_{011}) - (w_{100} + w_{101}) \\ u_{101} &= (w_{000} + w_{010}) + (w_{101} + w_{111}) - (w_{001} + w_{011}) - (w_{100} + w_{110}) \\ u_{011} &= (w_{000} + w_{100}) + (w_{011} + w_{111}) - (w_{001} + w_{101}) - (w_{010} + w_{110}) \\ u_{111} &= (w_{000} + w_{011} + w_{101} + w_{110}) - (w_{100} + w_{010} + w_{001} + w_{111}). \end{aligned}$$

These four linear forms form a natural basis for the interaction space $\mathcal{I}_{\{0,1\}^3}$. The interaction coordinate u_{110} measures the *marginal epistasis* between locus 1 and locus 2, and similarly for u_{101} and u_{011} . The last interaction coordinate u_{111} measures the *three-way interaction* among the loci.

The 3-cube has twenty circuits in three symmetry classes. We abbreviate the circuits of the 3-cube by the first twenty letters of the alphabet. The first six circuits corresponds to the six faces of the 3-cube, and they measure the *conditional epistasis* between two loci when the allele at the third locus is fixed:

$$\begin{aligned} a &:= u_{110} + u_{111} = w_{000} - w_{010} - w_{100} + w_{110} \\ b &:= u_{110} - u_{111} = w_{001} - w_{011} - w_{101} + w_{111} \\ c &:= u_{101} + u_{111} = w_{000} - w_{001} - w_{100} + w_{101} \\ d &:= u_{101} - u_{111} = w_{010} - w_{011} - w_{110} + w_{111} \\ e &:= u_{011} + u_{111} = w_{000} - w_{001} - w_{010} + w_{011} \\ f &:= u_{011} - u_{111} = w_{100} - w_{101} - w_{110} + w_{111}. \end{aligned}$$

The second class of circuits relates marginal epistases of two pairs of loci:

$$\begin{aligned} g &:= u_{110} + u_{101} = w_{000} - w_{011} - w_{100} + w_{111} \\ h &:= u_{110} - u_{101} = w_{001} - w_{010} - w_{101} + w_{110} \\ i &:= u_{110} + u_{011} = w_{000} - w_{010} - w_{101} + w_{111} \\ j &:= u_{110} - u_{011} = w_{001} - w_{011} - w_{100} + w_{110} \\ k &:= u_{101} + u_{011} = w_{000} - w_{001} - w_{110} + w_{111} \\ l &:= u_{101} - u_{011} = w_{010} - w_{011} - w_{100} + w_{101}. \end{aligned}$$

Geometrically, the six circuits $g, h, i, j, k,$ and l correspond to squares formed by vertices of the 3-cube that slice the 3-cube into two triangular prisms.

The last class consists of eight circuits which relate the three-way interaction

to the total two-way epistasis, where signs are taken into consideration:

$$\begin{aligned}
m &:= -u_{011} - u_{101} - u_{110} - u_{111} = w_{001} + w_{010} + w_{100} - w_{111} - 2w_{000} \\
n &:= -u_{011} - u_{101} - u_{110} + u_{111} = w_{011} + w_{101} + w_{110} - w_{000} - 2w_{111} \\
o &:= u_{011} + u_{101} - u_{110} - u_{111} = w_{010} + w_{100} + w_{111} - w_{001} - 2w_{110} \\
p &:= u_{011} + u_{101} - u_{110} + u_{111} = w_{000} + w_{011} + w_{101} - w_{110} - 2w_{001} \\
q &:= u_{011} - u_{101} + u_{110} - u_{111} = w_{001} + w_{100} + w_{111} - w_{010} - 2w_{101} \\
r &:= u_{011} - u_{101} + u_{110} + u_{111} = w_{000} + w_{011} + w_{110} - w_{101} - 2w_{010} \\
s &:= -u_{011} + u_{101} + u_{110} + u_{111} = w_{000} + w_{101} + w_{110} - w_{011} - 2w_{100} \\
t &:= -u_{011} + u_{101} + u_{110} - u_{111} = w_{001} + w_{010} + w_{111} - w_{100} - 2w_{011}.
\end{aligned}$$

Geometrically, these correspond to the eight bipyramids in the 3-cube. \square

The sign of the interaction coordinate u in the two locus case of Example 3.7 determines the nature of the epistatic interaction. In the three-locus case, one may wish to record the signs of each of the twenty circuits a, b, \dots, t . For instance, the signs of a, b, c, d, e , and f specify all the conditional epistases of the fitness landscape w . The signs of the bipyramidal circuits m, n, \dots, t describe a three-way interaction which does not have a two-locus interpretation. The complete list of the twenty signs characterizes all the interactions among the genotypes, and also determines (but is not equivalent to) the shape of the fitness landscape. This is made precise in Proposition 4.13.

While the detailed study of the n -cube for small values of n provides a useful tool for data analysis, we wish to recall that biological genotypes may not be cubes. In such cases, there may not be any choice of interaction coordinates which is as nice and canonical as that coming from the Fourier transform. Fixing a basis for the interaction space will be a matter of choice and preference. What remains canonical and natural is the full collection of all circuits of the genotype.

We conclude our discussion of gene interactions by comparing the proposed circuits to the more traditional approach of using ANOVA (Lindman, 1974). We illustrate the key difference between the two methods in the following example.

Example 3.10. (Two DNA loci) Consider the genotype space $\mathcal{G} = \{\mathbf{A}, \mathbf{C}, \mathbf{G}$,

$\mathbb{T}\}^2$ of two DNA loci. A fitness landscape on \mathcal{G} is a matrix

$$w = \begin{pmatrix} w_{AA} & w_{AC} & w_{AG} & w_{AT} \\ w_{CA} & w_{CC} & w_{CG} & w_{CT} \\ w_{GA} & w_{GC} & w_{GG} & w_{GT} \\ w_{TA} & w_{TC} & w_{TG} & w_{TT} \end{pmatrix}.$$

Let $\bar{w}_{i\bullet}$ and $\bar{w}_{\bullet j}$ denote the row and column means, respectively, of w , and denote by $\bar{w}_{\bullet\bullet}$ the grand mean. In the 2-way ANOVA analysis of the table w , one considers the 16 linear forms

$$w_{ij} - \bar{w}_{i\bullet} - \bar{w}_{\bullet j} + \bar{w}_{\bullet\bullet} \quad (i, j \in \{\mathbf{A}, \mathbf{C}, \mathbf{G}, \mathbf{T}\}),$$

which measure the direction and amount by which each fitness value differs from our expectation based only on the row and column means. By contrast, there are 204 circuits in the interaction space $\mathcal{I}_{\mathcal{G}}$, including, for example,

$$\begin{aligned} & w_{AG} - w_{AT} - w_{TG} + w_{TT}, \\ & -w_{AC} + w_{AG} + w_{CA} - w_{CT} - w_{GG} + w_{GT} - w_{TA} + w_{TC}, \\ & -w_{AA} + w_{AG} - w_{GG} + w_{GT} + w_{TA} - w_{TT}. \end{aligned}$$

Thus, the circuits measure deviation from linearity in a different, much finer way than ANOVA does. \square

4. The Shapes of Fitness Landscapes

We have defined fitness landscapes as discrete objects that assign one fitness value to each individual genotype $g \in \mathcal{G}$. However, in order to speak about “shape” or “curvature” of $w : \mathbb{R} \rightarrow \mathcal{G}$, one needs a continuous object. This dilemma is resolved by considering populations $p \in \Delta_{\mathcal{G}}$ rather than individuals.

The fitness of a population p is defined as the average fitness of all individuals in the population. Since the individuals are grouped into classes of identical genotypes, the population fitness can be written as the dot product

$$w \cdot p = \sum_{g \in \mathcal{G}} w_g \cdot p_g.$$

This notion of population fitness leads to an extension of a discrete landscape $w : \mathcal{G} \rightarrow \mathbb{R}$ to a function \tilde{w} on the full genotype $\Pi_{\mathcal{G}}$. The *continuous landscape*

$\tilde{w}: \Pi_{\mathcal{G}} \rightarrow \mathbb{R}$ derived from w assigns to each point v in the genotope the maximum fitness among all populations p with these allele frequencies. We define

$$\tilde{w}(v) := \max \{p \cdot w : p \in \rho^{-1}(v)\} \quad \text{for all } v \in \Pi_{\mathcal{G}}. \quad (4.1)$$

Computing the fitness value $\tilde{w}(v)$ amounts to solving a $c(\mathcal{G})$ -dimensional linear programming problem, namely, to maximizing the linear functional $p \mapsto p \cdot w$ over the fiber $\rho^{-1}(v)$. The continuous landscape \tilde{w} is the smallest convex function which has the same values as w on the vertices of $\Pi_{\mathcal{G}}$. It is continuous and piecewise linear. Our classification of landscapes rests on the following remark.

Remark 4.11. *The domains of linearity of the piecewise linear function \tilde{w} are the cells in a regular polyhedral subdivision $\Pi_{\mathcal{G}}[w]$ of the genotope $\Pi_{\mathcal{G}}$.*

We refer to the book of De Loera et al. (2006) for an introduction to the geometry of polyhedral subdivisions. Remark 4.11 appears in (De Loera et al., 2006, Chap. 2). We call the induced polyhedral subdivision $\Pi_{\mathcal{G}}[w]$ the *shape* of the fitness landscape w . For almost all fitness landscapes $w \in \mathbb{R}^{\mathcal{G}}$, the subdivision $\Pi_{\mathcal{G}}[w]$ will be a *regular triangulation*, i.e., a subdivision all of whose cells are simplices. We call such landscapes *generic fitness landscapes*.

The simplices in the triangulation $\Pi_{\mathcal{G}}[w]$ have a natural interpretation in terms of populations. For any n -tuple of allele frequencies $v \in \Pi_{\mathcal{G}}$, there is a unique fittest population p with $\rho(p) = v$. The genotypes that occur in this fittest population are the vertices of the simplex of $\Pi_{\mathcal{G}}[w]$ which contains v . Thus, knowing the shape of a fitness landscape w is equivalent to knowing all the fittest populations for w . For instance, in Example 3.7, if w has positive epistasis, then 01 and 10 cannot coexist in a fittest population, so any fittest population consists either of genotypes in the triangle $\{00, 01, 11\}$ or of genotypes in $\{00, 10, 11\}$.

The number of shapes of fitness landscapes on a fixed genotype space \mathcal{G} is finite. If \mathcal{G} has few elements (say, less than twenty), then a complete list of all generic shapes can be compiled using the software TOPCOM (Rambau, 2002) which enumerates triangulations. For instance, the number of generic shapes of fitness landscapes on the cube $\{0, 1\}^n$ is two if $n = 2$, and it is 74 if $n = 3$ (Table 5.1). In Section 5, we discuss the 74 shapes of fitness landscapes on $\{0, 1\}^3$.

In order to classify all shapes of fitness landscapes on a genotype space \mathcal{G} , we need to list all polyhedral subdivisions of the genotope $\Pi_{\mathcal{G}}$. This set

of subdivisions is represented by the *secondary polytope* $\Sigma_{\mathcal{G}}$ (De Loera et al., 2006, Chap. 5). The secondary polytope $\Sigma_{\mathcal{G}}$ has dimension $c(\mathcal{G})$, it lives in the space dual to $\mathbb{R}^{\mathcal{G}}$, and its vertices are in bijection with the generic shapes. The higher-dimensional faces of the secondary polytope $\Sigma_{\mathcal{G}}$ correspond to non-generic shapes. Thus, the secondary polytope of a genotype space \mathcal{G} represents all shapes of fitness landscapes on \mathcal{G} and their neighborhood relations. In Example 3.7, the secondary polytope $\Sigma_{\mathcal{G}}$ is a line segment. Its two vertices correspond to the two generic shapes, and the segment itself corresponds to the flat shape.

In general, the secondary polytope can be defined as follows. Consider the average fitness of the fittest populations over all n -tuples of allele frequencies:

$$\mathbf{F}(w) = \frac{1}{\text{vol}(\Pi_{\mathcal{G}})} \cdot \int_{\Pi_{\mathcal{G}}} \tilde{w}(v) dv.$$

This integral is a piecewise linear function in the unknown fitness landscape $w \in \mathbb{R}^{\mathcal{G}}$. Two landscapes w and w' have the same generic shape precisely when they lie in a common domain of linearity of this piecewise-linear function. Thus for each generic shape, the function \mathbf{F} is represented by a linear functional on $\mathbb{R}^{\mathcal{G}}$, i.e., by a vector F in the dual space $(\mathbb{R}^{\mathcal{G}})^*$. The coordinate F_g of this vector with respect to the standard basis on $(\mathbb{R}^{\mathcal{G}})^*$, equals the probability that the genotype g appears in a fittest population. The secondary polytope $\Sigma_{\mathcal{G}}$ is the convex hull in $(\mathbb{R}^{\mathcal{G}})^*$ of these vectors F , one for each generic shape.

Example 4.12. Let $\mathcal{G} = \{000, 011, 100, 101, 110, 111\}$ be the genotype space in Example 2.2 and Figure 2.2. The two interaction coordinates are

$$\begin{aligned} x &= w_{100} + w_{111} - w_{101} - w_{110} \\ y &= w_{000} + w_{111} - w_{011} - w_{100}. \end{aligned}$$

The average fitness $\mathbf{F}(w)$ is the piecewise-linear function in the six fitness values $w_{000}, w_{011}, w_{100}, w_{101}, w_{110},$ and w_{111} . The function $\mathbf{F}(w)$ equals

$$\frac{1}{4} \cdot \max \left\{ \begin{array}{l} 2w_{000} + 4w_{011} + 4w_{100} + 2w_{101} + 2w_{110} + 2w_{111}, \\ 2w_{000} + 4w_{011} + 3w_{100} + 3w_{101} + 3w_{110} + w_{111}, \\ 3w_{000} + 3w_{011} + w_{100} + 4w_{101} + 4w_{110} + w_{111}, \\ 4w_{000} + 2w_{011} + w_{100} + 3w_{101} + 3w_{110} + 3w_{111}, \\ 4w_{000} + 2w_{011} + 2w_{100} + 2w_{101} + 2w_{110} + 4w_{111} \end{array} \right\}.$$

Using the interaction coordinates, the average fitness can be rewritten as follows:

$$\begin{aligned} \mathbf{F}(w) = & (1/4) \cdot \max\{0, x, 2x - y, x - 2y, -2y\} \\ & + w_{011} + w_{100} + (w_{000} + w_{101} + w_{110} + w_{111})/2. \end{aligned}$$

The five cases in this maximum correspond to the five possible shapes of the fitness landscape. The corresponding triangulations of $\Pi_{\mathcal{G}}$ are

$$\begin{aligned} & \{\{101, 111, 100, 011\}, \{110, 111, 100, 011\}, \{101, 000, 100, 011\}, \{110, 000, 100, 011\}\} \\ & \{\{101, 000, 100, 011\}, \{110, 000, 100, 011\}, \{110, 101, 100, 011\}, \{110, 101, 111, 011\}\} \\ & \{\{110, 101, 111, 011\}, \{110, 101, 000, 100\}, \{110, 101, 000, 011\}\}_{\text{has volume 2}} \\ & \{\{110, 101, 000, 100\}, \{110, 101, 000, 111\}, \{101, 000, 111, 011\}, \{110, 000, 111, 011\}\} \\ & \{\{101, 000, 111, 100\}, \{110, 000, 111, 100\}, \{101, 000, 111, 011\}, \{110, 000, 111, 011\}\}. \end{aligned}$$

The secondary polytope $\Sigma_{\mathcal{G}}$ is a pentagon whose vertices are labeled by the five triangulations. It is represented geometrically as the pentagon in the interaction space $\mathcal{I}_{\mathcal{G}}$ whose directed edges are x , $x - y$, $-x - y$, $-x$, and $2y$. See Figure 6.6 for an illustration of the pentagon $\Sigma_{\mathcal{G}}$ in the context of HIV fitness data. \square

We now explain the relationship between the shapes of fitness landscapes on \mathcal{G} and the circuits in the interaction space $\mathcal{I}_{\mathcal{G}}$. We define the *circuit sign pattern* of a fitness landscape $w \in \mathbb{R}^{\mathcal{G}}$ to be the list which records the sign (positive, zero or negative) of the numerical value of each circuit at w .

Proposition 4.13. *The shape $\Pi_{\mathcal{G}}[w]$ of a fitness landscape $w \in \mathbb{R}^{\mathcal{G}}$ is determined by its circuit pattern, but the converse generally does not hold.*

Proof. Both the circuit sign patterns and the shapes define a subdivision of $\mathbb{R}^{\mathcal{G}}$ into cones which fit together to form a fan. This ensures that we need only consider the generic case when all circuits are either positive or negative at w . Each such linear inequality can be written in the form

$$\sum_{g \in \mathcal{G}_1} \alpha_g w_g > \sum_{g \in \mathcal{G}_2} \beta_g w_g,$$

where \mathcal{G}_1 and \mathcal{G}_2 are disjoint subsets of \mathcal{G} , and the α_g and β_g are positive reals. The genotypes in \mathcal{G}_2 cannot coexist in a fittest population, since they can be replaced by the genotypes in \mathcal{G}_1 , thus increasing population fitness while keeping the allele frequencies unchanged. Containing such a replaceable set \mathcal{G}_1 is the only

obstruction to being a simplex in the triangulation $\Pi_{\mathcal{G}}[w]$. In other words, the sets \mathcal{G}_1 derived from circuits as above are the minimal non-faces of the triangulation $\Pi_{\mathcal{G}}[w]$. This proves that $\Pi_{\mathcal{G}}[w]$ is determined by the circuit sign patterns at w .

The second part of the proposition follows from Figure 6.6, There are precisely four circuits, namely, $x, y, x+y, x-y$, and hence eight possible $\{+/-\}$ -sign patterns. The eight sign patterns map correspond to only five distinct shapes. \square

5. Three-way Interactions

We illustrate our generalization of the classical two-locus two-allele situation (Figure 1.1) by examining the possible fitness shapes for three biallelic loci. Here, the genotype space is $\mathcal{G} = \{000, 001, 010, 011, 100, 101, 110, 111\}$, and the possible fitness shapes are exactly the 74 triangulations of the 3-cube (Table 5.1).

Each triangulation is uniquely represented by its *GKZ vector* (De Loera et al., 2006), which is the vector $F \in (\mathbb{R}^{\mathcal{G}})^*$ introduced prior to Example 4.12. The GKZ vector indicates for each vertex $g \in \mathcal{G}$ the sum of the normalized volumes of all tetrahedra in the given triangulation that contain g . Equivalently, if the allele frequency vector is chosen uniformly at random from $\Pi_{\mathcal{G}}$, then the g -th entry of the GKZ vector is the probability that genotype g appears in the fittest population. We refer to the shape of a fitness landscape for a three-locus two-allele system by its number (1 to 74) as appearing in the first column of Table 5.1.

The 74 shapes label the vertices of the secondary polytope $\Sigma_{\mathcal{G}}$ of the 3-cube and are listed in Table 5.1. As an example consider the 17th vertex of $\Sigma_{\mathcal{G}}$:

$$17/3 \quad 23346114 \quad 3e28\bar{7}51b54d.$$

This says that shape 17 has the GKZ vector $(2, 3, 3, 4, 6, 1, 1, 4)$. The third column says that shape 17 is adjacent to the shapes 3, 28, 51 and 54. The letters a, b, \dots, t refer to the list of circuits in Example 3.9. The GKZ vector $(2, 3, 3, 4, 6, 1, 1, 4)$ differs from the GKZ vector of shape 3 by the circuit

$$e = u_{011} + u_{111} = w_{000} - w_{001} - w_{010} + w_{011} = (1, -1, -1, 1, 0, 0, 0, 0).$$

Similarly, shape 17 differs from shape 28 by the circuit $-g = -u_{110} - u_{101}$, from shape 51 by the circuit $b = u_{110} - u_{111}$, and from shape 54 by the circuit $d = u_{101} - u_{111}$. The circuits e, b , and d measure conditional epistasis between

| #/T | GKZ | Out-edges | #/T | GKZ | Out-edges |
|------|----------|--------------|------|----------|--------------------|
| 1/1 | 15515115 | 3t4q5o6m | 38/4 | 31355313 | 39l44g51c59d |
| 2/1 | 51151551 | 7s8r9p10n | 39/4 | 31533513 | 38l44i53e60f |
| 3/2 | 14436114 | 1l11b13d17e | 40/4 | 33155133 | 42j45g54a61b |
| 4/2 | 14614314 | 1q12b14f18c | 41/4 | 33511533 | 43h46i55a62b |
| 5/2 | 16414134 | 1r15d16f19a | 42/4 | 35133153 | 40j45k57e63f |
| 6/2 | 34414116 | 1m28e29c31a | 43/4 | 35311353 | 41h46k58c64d |
| 7/2 | 41163441 | 2s20a22c26f | 44/4 | 51333315 | 38g39i65b68a |
| 8/2 | 41341641 | 2r21a23e27d | 45/4 | 53133135 | 40g42k66d69c |
| 9/2 | 43141461 | 2p24c25e30b | 46/4 | 53311335 | 41i43k67f70e |
| 10/2 | 61141443 | 2n32f33d34b | 47/5 | 13356222 | 11d13b35f71e |
| 11/3 | 13446213 | 3b12l47d51e | 48/5 | 13623522 | 12f14b36d72c |
| 12/3 | 13624413 | 4b11l48f53c | 49/5 | 16323252 | 15f16d37b73a |
| 13/3 | 14346123 | 3d15j47b54e | 50/5 | 22265331 | 20c22a35e71f |
| 14/3 | 14613423 | 4f16h48b55c | 51/5 | 22356213 | 11e17b38c71d |
| 15/3 | 16324143 | 5d13j49f57a | 52/5 | 22532631 | 21e23a36c72d |
| 16/3 | 16413243 | 5f14h49d58a | 53/5 | 22623513 | 12c18b39e72f |
| 17/3 | 23346114 | 3e28g51b54d | 54/5 | 23256123 | 13e17d40a71b |
| 18/3 | 23613414 | 4c29i53b55f | 55/5 | 23612523 | 14c18f41a72b |
| 19/3 | 26313144 | 5a31k57d58f | 56/5 | 25232361 | 24e25c37a73b |
| 20/3 | 31264431 | 7a21l50c59f | 57/5 | 26223153 | 15a19d43e73f |
| 21/3 | 31442631 | 8a20l52e60d | 58/5 | 26312253 | 16a19f43e73d |
| 22/3 | 32164341 | 7c24j50a61f | 59/5 | 31265322 | 20f26a38d71c |
| 23/3 | 32431641 | 8e25h52a62d | 60/5 | 31532622 | 21d27a39f72e |
| 24/3 | 34142361 | 9c22j56e63b | 61/5 | 32165232 | 22f26c40b71a |
| 25/3 | 34231461 | 9e23h56c64b | 62/5 | 32521632 | 23d27e41b72a |
| 26/3 | 41164332 | 7f32g59a61c | 63/5 | 35132262 | 24b30c42f73e |
| 27/3 | 41431632 | 8d33i60a62e | 64/5 | 35221362 | 25b30e32d73c |
| 28/3 | 43324116 | 6e17g65c66a | 65/5 | 52323216 | 28c29e44b74a |
| 29/3 | 43413216 | 6c18i65e67a | 66/5 | 53223126 | 28a31e45d74c |
| 30/3 | 44131362 | 9b34k63c64e | 67/5 | 53312226 | 29a31c46f74e |
| 31/3 | 44313126 | 6a19k66e67c | 68/5 | 61232325 | 32d33f44a74b |
| 32/3 | 61142334 | 10f26g68d69b | 69/5 | 62132235 | 32b34f45c74d |
| 33/3 | 61231434 | 10d27i68f70b | 70/5 | 62221335 | 33b34d46e74f |
| 34/3 | 62131344 | 10b30k69f70d | 71/6 | 22266222 | 47e50f51d54b59c61a |
| 35/4 | 13355331 | 36l37j47f50e | 72/6 | 22622622 | 48c52d53f55b60e62a |
| 36/4 | 13533531 | 35l37h48d52c | 73/6 | 26222262 | 49a56b57f58d63e64c |
| 37/4 | 15333351 | 35j36h49b56a | 74/6 | 62222226 | 65a66c67e68b69d70f |

Table 5.1: The 74 shapes of fitness landscapes of the three-locus two-allele system. The first column specifies the shape number and type, the second column the GKZ vector, and the third column the out-edges in the secondary polytope.

two loci when the third is fixed, so the secondary polytope tells us, for example, that shapes 17 and 51 differ only by such a conditional epistasis interaction.

In the first column of Table 5.1, one more number of interest is displayed after the shape number and separated by a slash, namely the *interaction type*. Shapes of the same interaction type differ only in the labeling of the vertices of the cube; in other words, they correspond to the same combinatorial type of triangulation. The six interaction types correspond to the six symmetry classes of triangulations of the 3-cube. These six classes are depicted in (De Loera et al., 2006, Fig. 1.38) and in (Grier et al., 2006, Fig. 1), and we refer to these references for further mathematical background and generalizations to higher dimensions.

Table 5.1 specifies all the shapes of fitness landscapes for three biallelic loci. It is useful to examine the six interaction types, and to consider their biological meaning. The two triangulations of type 1 are obtained if the three-way interaction u_{111} is either very large or very small. It consists of a central tetrahedron of volume two and four adjacent tetrahedra of volume one. The central tetrahedron can either use the genotypes with an even number of mutations, or those with an odd mutation count. Fitness landscapes of this type are linear on the central tetrahedron and on the adjacent tetrahedra. The curvature is such that fitness decreases more strongly than expected towards any of the genotypes that are not part of the central tetrahedron. These four genotypes are “sliced off”, and the fittest populations avoid these genotypes whenever possible. Thus, the shape being of type 1 means that the fittest populations include either all genotypes with an even number of mutations, or all genotypes with an odd number of mutations.

Type 6 landscapes can be regarded as opposite to type 1. The four triangulations of this type are indexed by the four different diagonals of the 3-cube. Each diagonal induces a triangulation that consists of six tetrahedra arranged around the diagonal in such a way that each tetrahedron has exactly two adjacent tetrahedra. Fitness landscapes of this type are linear on each tetrahedron and the curvature is such that any of the six tetrahedra has a higher fitness than expected from its two neighbors. No single genotypes are sliced off, as all entries of the GKZ vector are bigger than 1. For example, shape 74 uses the diagonal through 000 and 111. Hence the vertices of the tetrahedra correspond to different accumulative mutational pathways of length four from 000 to 111. For example,

000 \rightarrow 001 \rightarrow 101 \rightarrow 111 is one such pathway. Thus, the fittest populations involve all genotypes from exactly one of the six possible pathways.

Types 1 and 6 represent the two extreme types of three-way interaction. Type 1 emphasizes the number of mutations irrespective of the particular context or pathway they occur in. By contrast, type 6 emphasizes the mutational pathway. Type 1 fitness shapes occur when intermediate types are fitter than expected irrespective of the specific intermediate genotype. Likewise, we expect type 6 fitness shapes whenever higher fitness values than expected occur only in specific genotypic contexts. The remaining interaction types (2 to 5) are intermediate and share features from both type 1 and type 6.

It is important to note that the third column in Table 5.1 gives the minimal set of linear inequalities that characterize the *robustness cone* for each of the 74 shapes. These cones consist of all fitness landscapes that have the given shape. For instance, shape 74 is characterized by the inequalities $a, b, c, d, e, f > 0$ which says that conditional epistasis is positive for any fixation of one of the three loci. While type 6 requires six inequalities, each of the other five types requires only four. For instance, being in shape 38 means that the conditional epistases c and d are positive while the marginal epistases g and l are negative.

For the four-locus two-allele system ($\mathcal{G} = \{0, 1\}^4$), it was shown by Grier et al. (2006) that the number of shapes is 87,959,448, and that these fall into 235,277 symmetry types. A table analogous to Table 5.1, listing one representative shape from each type, is available at <http://bio.math.berkeley.edu/4cube/>.

6. Positive Epistasis in HIV?

In this section, we characterize the fitness landscape of HIV-1. We use the data published in (Segal et al., 2004), which is also described in (Bonhoeffer et al., 2004). The data consists of 288 genotype–fitness pairs. The reported genotype is the HIV protein sequence composed of positions 4 to 99 of the protease (PRO) and positions 38 to 223 of the reverse transcriptase (RT). Fitness was measured as the number of offspring in a single replication cycle and was reported relative to the fixed wild type strain NL4-3 on a logarithmic scale. Univariate and multivariate analyses show that mutation L90M in the protease, and mutations M184V and T215Y in the RT are the major determinants of fitness in this data set. The notation L90M means that at position 90, the amino acid leucine (L) is

| Genotype | Count | Min. | 1st Qu. | Median | Mean | 3rd Qu. | Max. |
|----------|-------|---------|---------|--------|---------------|---------|--------|
| 000 | 214 | 0.1917 | 1.4770 | 1.6410 | 1.5800 | 1.7910 | 2.0530 |
| 001 | 5 | 0.5344 | 0.6990 | 1.1880 | 1.1950 | 1.7710 | 1.7850 |
| 010 | 8 | -0.3355 | 1.1440 | 1.2960 | 1.1330 | 1.4870 | 1.5310 |
| 011 | 8 | 1.0000 | 1.2500 | 1.5150 | 1.4300 | 1.6360 | 1.7240 |
| 100 | 7 | 0.4771 | 1.3470 | 1.4650 | 1.4410 | 1.7890 | 1.8750 |
| 101 | 13 | 0.3010 | 0.8673 | 1.3420 | 1.2320 | 1.5840 | 1.8870 |
| 110 | 11 | 0.6021 | 1.1610 | 1.3700 | 1.2940 | 1.5370 | 1.6920 |
| 111 | 22 | -0.4771 | 0.9472 | 1.1790 | 1.0450 | 1.3850 | 1.7900 |

Table 6.2: HIV random fitness landscape on the three amino acid mutations PRO L90M, RT M184V, and RT T215Y. The mean values (in bold) are used for significance testing.

replaced by methionine (M). We therefore analyze the fitness shape of this three-locus two-allele system. We identify the subsets of {L90M, M184V, T215Y} with binary strings of length three. For instance, the string 010 in the third row in Table 6.2 is the genotype carrying only mutation M184V.

The fitness values were measured for different viruses, some of which share a mutational pattern on the three selected loci. Thus, instead of a single fitness value for each genotype, we have a distribution. A *random fitness landscape* on a genotype space \mathcal{G} is a collection of $|\mathcal{G}|$ continuous random variables $W = (W_g)_{g \in \mathcal{G}}$. We think of a realization of W as a real-valued function $w: \mathcal{G} \rightarrow \mathbb{R}$ on the genotype space. Thus, W takes values in $\mathbb{R}^{\mathcal{G}}$. In general, stochastic fluctuations in W can arise from measurement noise in assessing the reproductive fitness experimentally and from biological variation that is not linked to the n genetic loci. The HIV random fitness landscape is summarized in Table 6.2.

Following Bonhoeffer et al. (2004) and Sanjuán et al. (2004), we first examine the total marginal two-way epistasis

$$E = u_{110} + u_{101} + u_{011},$$

with u_{ijk} defined in Example 3.9. Computing E means pooling epistasis estimates obtained from the three pairs of loci. We use randomized fitness values to estimate E under the null hypothesis of no epistasis. Unlike in (Bonhoeffer et al., 2004), we do not find the observed positive value of $\hat{E} = 0.025$ to be significantly greater than zero ($P > 0.35$). This discrepancy may reflect the limited statistical

| Circuit | Pair | Context | Cond. epist. | P -value |
|---------|---------|---------|--------------|------------|
| a | 90–184 | T215 | 0.300 | 0.110 |
| b | 90–184 | 215Y | −0.421 | 0.059 |
| c | 90–215 | M184 | 0.175 | 0.230 |
| d | 90–215 | 184V | −0.545 | 0.013 |
| e | 184–215 | L90 | 0.682 | 0.008 |
| f | 184–215 | 90M | −0.039 | 0.410 |

Table 6.3: Conditional 2-way epistasis in HIV. The P -value denotes the fraction of epistasis values in the bootstrap sample that are lower (in the case of negative epistasis) or higher (in the case of positive epistasis) than the observed mean conditional epistasis. Circuits are labeled as in Example 3.9.

power of our analysis, which is based on a smaller data set and on only 3 loci, although Bonhoeffer et al. found positive epistasis to be more pronounced when restricting to the most influential sequence positions.

Rather than marginalizing, we next consider two-way epistasis conditional on the value at the third locus, i.e., we determine the pattern of epistasis for each pair of loci in the context of the third locus (Table 6.3). For all three pairs, we find positive epistasis conditioned on the wild type allele at the third position, and negative conditional epistasis otherwise. Two out of six comparisons reached statistical significance, including one case of negative epistasis. Figure 6.4 shows the empirical null distributions (grey histogram bars) and, in addition, the empirical distributions of the circuits a , b , c , d , e , and f (as defined in Example 3.9) that represent conditional epistasis (clear histogram bars). The distributions of circuits are obtained by resampling fitness values for the same genotype. They reflect the uncertainty in the shape of the fitness landscape due to multiple discordant measurements. We conclude that the HIV fitness landscape on the three selected loci is insufficiently described as “positively epistatic”.

We now characterize the shape of the HIV fitness landscape by estimating the distribution on the 74 shapes in Table 5.1 induced by the data in Table 6.2. We use a resampling scheme to estimate the distribution and shape of W . The distribution of $\Pi_{\mathcal{G}}[W]$ is shown in Figure 6.5(a). The dominant shapes are #7 (frequency 20.9%), #2 (20.7%), #26 (15%), and #61 (11.3%). In Figure 6.5(b), we randomized the fitness values. Comparing the two histograms shows that the

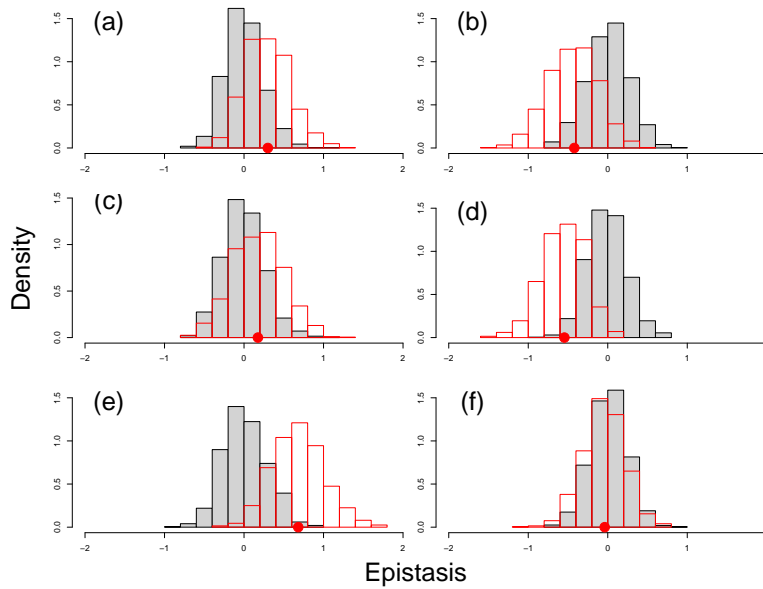


Figure 6.4: Conditional two-way epistasis in HIV, grouped according to circuits a, \dots, f .

observed shape distribution is very different from a randomly chosen landscape using the same values. The histogram in Figure 6.5(c) results from sampling fitness values uniformly at random from $[0, 1]$ and is similar to the one in subfigure (b). Figure 6.5 can be used to detect differences in fitness shape between random landscapes, and to identify single shapes that appear with high probability.

The dominant shapes of the HIV fitness landscape are very similar and have certain features in common. For example, the GKZ vectors that correspond to shapes 2, 7, 10, 26, and 32 all share a coordinate 1 in both the second and third position. These five shapes account for 61.5% of the probability mass. They all slice off the two genotypes 001 and 010, which correspond to the single mutants $\{M184V\}$ and $\{T215Y\}$, respectively. Both mutations are known to reduce the fitness of HIV. Indeed, M184V develops shortly after initiation of therapy with the antiviral drug lamivudine in most patients. Although M184V carrying viruses are resistant to lamivudine, administration of the drug is often continued in order to maintain the mutation and its fitness impairing effect (Wainberg, 2004).

This suggests studying the fitness landscape on the subset $\mathcal{G} = \{000, 110, 011, 100, 101, 111\}$. The secondary polytope of \mathcal{G} is a pentagon whose vertices

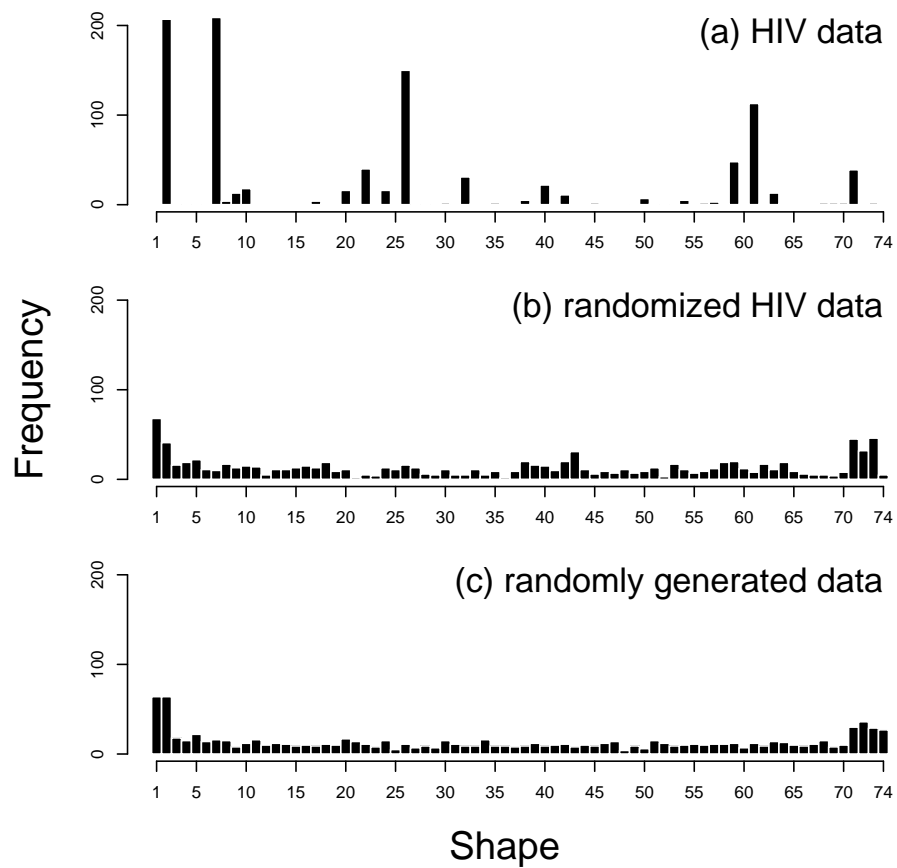


Figure 6.5: Three-way epistasis in HIV, analyzed using the 74 shapes in Table 5.1. Shape distribution of (a) the HIV random fitness landscape on mutations PRO L90M, RT M184V, and RT T215Y; (b) the same fitness values randomly assigned to genotypes; and (c) a random landscape in which fitness values are identically and uniformly distributed.

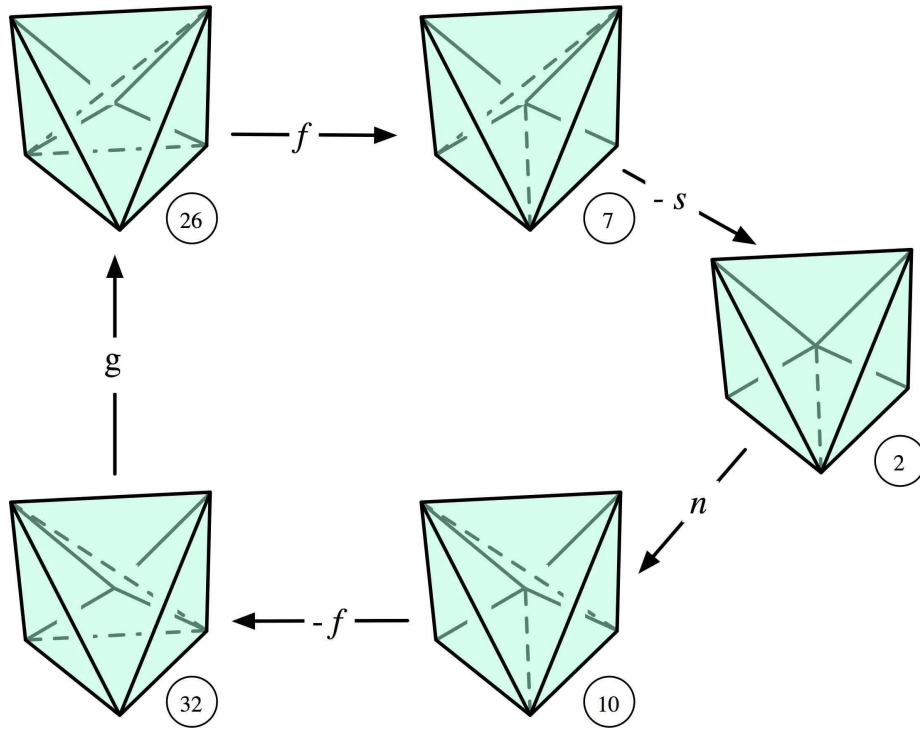


Figure 6.6: The secondary polytope of the genotype in Figure 2.2. It appears as a face of the secondary polytope of the 3-cube and its vertices and edges are labeled as in Table 5.1. The underlying genotype space is defined in Example 2.2 and represents the HIV fitness landscape shapes that slice off the single mutants $\{M184V\}$ and $\{T215Y\}$.

correspond to the shapes 2, 7, 10, 26, and 32, i.e., the five triangulations of the genotope in Example 2.2 and Figure 2.2. Figure 6.6 shows this pentagon. Vertices and edges are labeled as in Table 5.1. The pentagon reveals that shapes 26 and 7, and 32 and 10, differ only by the circuit f . This circuit represents conditional epistasis between the two RT loci 184 and 215 in the context of the protease mutation 90M (Table 6.3, Figure 6.4f). The other edges are the circuits g , n , and s . The circuit g relates the marginal epistasis of the two pairs (PRO 90, RT 184) and (PRO 90, RT 215). The circuit n compares the total two-way epistasis E to the three-way interaction u_{111} , and s compares the epistasis in (RT 184, RT 215) to the remaining pairs plus the three-way interaction.

In summary, analysis of the HIV fitness data has revealed a specific pentagon in the boundary of the (four-dimensional) secondary polytope of the 3-cube. The three dominant shapes 7, 2, and 26 in the random fitness landscape are adjacent on the pentagon, and they correspond to three of the five triangulations of the genotope in Figure 2.2. This geometric characterization of the fitness landscape captures more adequately the interactions underlying the HIV fitness data.

7. Synergistic Epistasis in *Drosophila*

Turning to a higher-dimensional genetic system, this section illustrates our concepts and methods with the fitness data for *Drosophila melanogaster* reported by Whitlock and Bourguet (2000). Those authors considered five genetic loci, denoted px/sp , b , ca , e/sr and h , for which they created a set of $32 = 2^5$ homozygous lines fixed for all the possible different combinations of mutations. We characterize the shape of the fitness landscape they measured, and we discuss their statistical analysis in light of our findings. Here, $l = 2$ and the genotype space is $\mathcal{G} = \{0, 1\}^5$. The binary strings $g \in \mathcal{G}$ represent the subsets of $\{\text{px/sp}, \text{b}, \text{ca}, \text{e/sr}, \text{h}\}$. For instance, 01011 represents the mutant b/e/sr/h . In what follows, we list the elements of \mathcal{G} in the following order:

| | | | | | | | |
|-------|-------|-------|-------|-------|-------|-------|-------|
| 00000 | 10000 | 01000 | 00100 | 00010 | 00001 | 11000 | 10100 |
| 10010 | 10001 | 01100 | 01010 | 01001 | 00110 | 00101 | 00011 |
| 11100 | 11010 | 11001 | 10110 | 10101 | 10011 | 01110 | 01101 |
| 01011 | 00111 | 11110 | 11101 | 11011 | 10111 | 01111 | 11111 |

The first column in (Whitlock and Bourguet, 2000, Tab. 1) consists of the fitness

values w_{ijklm} which measure the relative reproductive fitness of each strain:

$$\begin{array}{cccccccc} -0.232 & -0.850 & -0.312 & -0.214 & -0.847 & 0.507 & -0.238 & -0.490 \\ -1.030 & 0.232 & -0.968 & -1.338 & -0.034 & -1.47 & -0.739 & 0.2176 \\ -0.712 & -1.820 & -0.529 & -0.786 & -0.195 & -0.641 & -1.945 & -0.047 \\ 0.0264 & -1.296 & -2.446 & -1.973 & -1.180 & -1.024 & -1.856 & -4.560 \end{array}$$

These values define the fitness landscape $w : \mathcal{G} \rightarrow \mathbb{R}$, e.g., $w_{01100} = -0.968$.

Whitlock and Bourguet’s analysis of epistasis begins with an examination of the ten two-way interactions. They find that six of the 10 pairs show significant interaction. In all of them the direction of the effect is negative (synergistic epistasis). As we show below, each of the two-way interactions depends on the genotypes at the remaining loci, and a refined analysis provides more information.

The shape $\Pi_{\mathcal{G}}[w]$ of the *Drosophila* fitness landscape is a triangulation of the 5-cube $\Pi_{\mathcal{G}}$. It consists of the 110 maximal simplices displayed in Figure 7.7. Although the figure does not convey an intuitive image of the shape, it precisely characterizes the interactions. For verification, we computed the triangulation twice, once using the computer algebra software `Macaulay 2` (Grayson and Stillman, 1999) and once using the geometry software `Polymake` (Gawrilow and Joswig, 2001), both in less than one second running time on a standard PC.

Returning to the question of synergistic epistasis, we examine each pair of loci when we fix the values (0 or 1) at the remaining three loci. For example, the first pair of loci (1, 2) (i.e., (px/sp, b)) has positive epistasis twice, namely when there is either no other mutation or only the mutation 3 (ac). However, as soon as either of mutations 4 (e/sr) or 5 (h) occurs, the epistasis between px/sp and b becomes negative. Algebraically, if we write

$$\alpha_{**klm} = w_{00klm} + w_{11klm} - w_{01klm} - w_{10klm}$$

then $\alpha_{**000} = 0.692$ and $\alpha_{**100} = 0.532$ are positive while the other six epistatic interactions have negative numerical values:

$$\begin{array}{lll} \alpha_{**001} = -0.220 & \alpha_{**010} = -0.299 & \alpha_{**011} = -0.3478 \\ \alpha_{**101} = -2.470 & \alpha_{**110} = -1.185 & \alpha_{**111} = -2.976. \end{array}$$

Biologically, this analysis confirms the negative total marginal two-way epistasis described in (Whitlock and Bourguet, 2000), however it also reveals precise information about the conditional epistasis. Geometrically, an analysis of all two-way

```

{00000, 00001, 00011, 00100, 01000, 11000}{00000, 00001, 00011, 00100, 10001, 11000}
{00000, 00010, 00011, 00100, 01000, 11000}{00000, 00010, 00011, 00100, 10110, 11000}
{00000, 00010, 00011, 10010, 10110, 11000}{00000, 00011, 00100, 10001, 10100, 11000}
{00000, 00011, 00100, 10100, 10110, 11000}{00000, 00011, 10001, 10010, 10110, 11000}
{00000, 00011, 10001, 10100, 10110, 11000}{00000, 10000, 10001, 10010, 10100, 11000}
{00000, 10001, 10010, 10100, 10110, 11000}{00001, 00011, 00100, 00101, 01101, 10101}
{00001, 00011, 00100, 01000, 01011, 11000}{00001, 00011, 00100, 01011, 01101, 11000}
{00001, 00011, 00100, 01101, 10001, 10101}{00001, 00011, 00100, 01101, 10001, 11000}
{00001, 00011, 01011, 01101, 10001, 11000}{00001, 00100, 01000, 01011, 01101, 11000}
{00001, 01000, 01001, 01011, 01101, 11000}{00001, 01001, 01011, 01101, 10001, 11000}
{00010, 00011, 00100, 00110, 01011, 10110}{00010, 00011, 00100, 01000, 01011, 10110}
{00010, 00011, 00100, 01000, 10110, 11000}{00010, 00011, 01000, 01011, 10110, 11000}
{00010, 00011, 01011, 10010, 10110, 11000}{00010, 00100, 00110, 01011, 01110, 10110}
{00010, 00100, 01000, 01010, 01011, 10110}{00010, 00100, 01010, 01011, 01110, 10110}
{00010, 01000, 01010, 01011, 10110, 11000}{00010, 01010, 01011, 10010, 10110, 11000}
{00011, 00100, 00101, 00111, 01101, 10101}{00011, 00100, 00110, 00111, 01101, 10110}
{00011, 00100, 00110, 01011, 01101, 10110}{00011, 00100, 00111, 01101, 10101, 10111}
{00011, 00100, 00111, 01101, 10110, 10111}{00011, 00100, 01000, 01011, 10110, 11000}
{00011, 00100, 01011, 01101, 10110, 11000}{00011, 00100, 01101, 10001, 10100, 10101}
{00011, 00100, 01101, 10001, 10100, 11000}{00011, 00100, 01101, 10100, 10101, 10110}
{00011, 00100, 01101, 10100, 10110, 11000}{00011, 00100, 01101, 10101, 10110, 10111}
{00011, 00110, 00111, 01011, 01101, 10110}{00011, 00111, 01011, 01101, 10110, 10111}
{00011, 01011, 01101, 10001, 10101, 10110}{00011, 01011, 01101, 10001, 10110, 11000}
{00011, 01011, 01101, 10101, 10110, 10111}{00011, 01011, 10001, 10011, 10110, 10111}
{00011, 01011, 10001, 10011, 10110, 11000}{00011, 01011, 10001, 10101, 10110, 10111}
{00011, 01011, 10010, 10011, 10110, 11000}{00011, 01101, 10001, 10100, 10101, 10110}
{00011, 01101, 10001, 10100, 10110, 11000}{00011, 10001, 10010, 10011, 10110, 11000}
{00100, 00110, 01011, 01101, 01110, 10110}{00100, 01000, 01010, 01011, 01110, 10110}
{00100, 01000, 01011, 01100, 01101, 11100}{00100, 01000, 01011, 01100, 01110, 10110}
{00100, 01000, 01011, 01100, 10110, 11100}{00100, 01000, 01011, 01101, 11000, 11100}
{00100, 01000, 01011, 10110, 11000, 11100}{00100, 01011, 01100, 01101, 01110, 10110}
{00100, 01011, 01100, 01101, 10110, 11100}{00100, 01011, 01101, 10110, 11000, 11100}
{00100, 01101, 10100, 10110, 11000, 11100}{00110, 00111, 01011, 01101, 01110, 10110}
{00111, 01011, 01101, 01110, 01111, 10110}{00111, 01011, 01101, 01111, 10110, 10111}
{01000, 01010, 01011, 01110, 10110, 11100}{01000, 01010, 01011, 10110, 11000, 11100}
{01000, 01011, 01100, 01110, 10110, 11100}{01001, 01011, 01101, 10001, 11000, 11001}
{01010, 01011, 01110, 10110, 11010, 11100}{01010, 01011, 10010, 10110, 11000, 11010}
{01010, 01011, 10110, 11000, 11010, 11100}{01011, 01100, 01101, 01110, 10110, 11100}
{01011, 01101, 01110, 01111, 10110, 11110}{01011, 01101, 01110, 10110, 11100, 11110}
{01011, 01101, 01111, 10110, 10111, 11110}{01011, 01101, 01111, 10111, 11011, 11110}
{01011, 01101, 10001, 10101, 10110, 11000}{01011, 01101, 10001, 10101, 11000, 11001}
{01011, 01101, 10101, 10110, 10111, 11100}{01011, 01101, 10101, 10110, 11000, 11100}
{01011, 01101, 10101, 10111, 11011, 11100}{01011, 01101, 10101, 11000, 11001, 11100}
{01011, 01101, 10101, 11001, 11011, 11100}{01011, 01101, 10110, 10111, 11100, 11110}
{01011, 01101, 10111, 11011, 11100, 11110}{01011, 01110, 10110, 11010, 11100, 11110}
{01011, 10001, 10011, 10110, 10111, 11011}{01011, 10001, 10011, 10110, 11000, 11011}
{01011, 10001, 10101, 10110, 10111, 11011}{01011, 10001, 10101, 10110, 11000, 11011}
{01011, 10001, 10101, 11000, 11001, 11011}{01011, 10010, 10011, 10110, 11000, 11011}
{01011, 10010, 10110, 11000, 11010, 11011}{01011, 10101, 10110, 10111, 11011, 11100}
{01011, 10101, 10110, 11000, 11011, 11100}{01011, 10101, 11000, 11001, 11011, 11100}
{01011, 10110, 10111, 11011, 11100, 11110}{01011, 10110, 11000, 11010, 11011, 11100}
{01011, 10110, 11010, 11011, 11100, 11110}{01101, 01111, 10111, 11011, 11101, 11110}
{01101, 10001, 10100, 10101, 10110, 11000}{01101, 10100, 10101, 10110, 11000, 11100}
{01101, 10101, 10111, 11011, 11100, 11101}{01101, 10101, 11001, 11011, 11100, 11101}
{01101, 10111, 11011, 11100, 11101, 11110}{01111, 10111, 11011, 11101, 11110, 11111}

```

Figure 7.7: The shape of the *Drosophila* fitness landscape.

interactions involves examining the 80 two-dimensional faces of the 5-cube. Of these 80 squares, we find that precisely 26 have positive epistasis. We list the numerical values of the 26 positive interactions grouped by pairs of loci:

$$(1,2) \alpha_{**000} = 0.692, \alpha_{**100} = 0.532,$$

$$(1,3) \alpha_{*0*00} = 0.342, \alpha_{*0*01} = 0.819, \alpha_{*0*10} = 0.867, \alpha_{*0*11} = 1.1306, \alpha_{*1*00} = 0.182,$$

$$(1,4) \alpha_{*00*0} = 0.435, \alpha_{*01*0} = 0.960,$$

$$(1,5) \alpha_{*000*} = 0.343, \alpha_{*010*} = 0.820,$$

$$(2,3) \alpha_{0**01} = 1.233, \alpha_{0**10} = 0.016,$$

$$(2,4) \alpha_{0*0*1} = 0.3498, \alpha_{0*1*0} = 0.279, \alpha_{1*0*1} = 0.222,$$

$$(2,5) \alpha_{0*01*} = 0.2998, \alpha_{0*10*} = 1.446, \alpha_{1*01*} = 0.251,$$

$$(3,4) \alpha_{01**0} = 0.049, \alpha_{10**1} = 0.044,$$

$$(3,5) \alpha_{01*0*} = 0.643,$$

$$(4,5) \alpha_{000**} = 0.3256, \alpha_{001**} = 0.699, \alpha_{010**} = 1.0864, \alpha_{110**} = 0.931.$$

Considering that $54/80 = 0.675$ is higher than the fraction 0.6 of negative two-way interactions identified by Whitlock and Bourguet, and that many of the positive epistatic interactions are very small, one can argue a stronger case for synergistic epistasis. Importantly, our analysis also reveals exactly which pairs of loci can have positive or negative epistasis, and how this depends on the patterns at the other loci. The pair (1,3) (i.e., (**px/sp**, **ca**)) has the largest number of positive epistasis patterns, namely five, while the pair (3,5) (i.e., (**ca**, **h**)) has only one. In order to assess the statistical significance of these interactions, it is imperative to have replicates of the fitness measurements (cf. Section 6).

The shape of the fitness landscape also reveals information about the fittest population. To see this, we return to the geometry in Figure 7.7. The polyhedral complex dual to the triangulation, is referred to as the *tight span* (Grier et al., 2006). For our data, the tight span is three-dimensional, with f-vector $(110, 214, 127, 22)$. Besides the 22 three-dimensional cells, the tight span of $\Pi_{\mathcal{G}}[w]$

has ten maximal cells of dimension 2 and two maximal cells of dimension one. These two “tentacles” correspond to the genotypes 10000 and 11111 which are “sliced off” in the triangulation, i.e., each of them lies in only one maximal simplex. The GKZ vector of the triangulation $\Pi_{\mathcal{G}}[w]$ equals $1/120$ times

$$\begin{pmatrix} 12, & 1, & 21, & 46, & 13, & 13, & 64, & 17, \\ 12, & 35, & 7, & 10, & 3, & 7, & 2, & 51, \\ 33, & 7, & 7, & 83, & 30, & 7, & 15, & 64, \\ 80, & 9, & 12, & 5, & 24, & 22, & 7, & 1 \end{pmatrix}$$

Recall that the entry of this vector indexed by genotype $g \in \mathcal{G}$ is the probability that g appears in the fittest population for a randomly chosen allele frequency vector. For instance, for the strain $10110 = \text{px/sp/ca/e/sr}$ that probability is $83/120 = 69.2\%$. The triangulation $\Pi_{\mathcal{G}}[w]$ can also be written in a way which is complementary to the list of 110 maximal simplices. Namely, there are 332 minimal non-faces of $\Pi_{\mathcal{G}}[w]$, 31 non-triangles, and the one non-tetrahedron

$$\{00100, 00010, 11000, 01011\}.$$

The shape of the fitness landscape implies that these four *Drosophila* mutants cannot coexist in a maximally fit population, however any three of them can.

8. Discussion

Our description of the shape of fitness landscapes in terms of triangulations of the genotype directly reveals information about all the interactions among the genotypes. In the case of many organisms, including humans, polymorphism occurs at single nucleotides in the genome (SNPs), and is usually of two types. Thus, even though humans are diploid, and in principle there could be 16 possible alleles at a polymorphic site, there are usually only $l = 2$. It is important to note that even though the number of SNPs is in the millions, the *human genotype* is determined only by the genotypes occurring in the population. The linkage disequilibrium structure of the human population (The International HapMap Consortium, 2005) suggests that the dimension of this genotype is far smaller than would be suggested by the number of SNPs. Thus, there is hope that in the future, with measurements of fitness one can learn about populations by examining the shapes of fitness landscapes on the human genotype. In the meantime, the

mathematics we have developed will be useful for studying interactions among genotypes in small mutation studies.

Another interpretation of the triangulations of the genotype is in terms of the genotypes that can occur in maximally fit populations. Such populations must consist of genotypes that label one simplex in the triangulation. In other words, the description of the shape of fitness landscapes that we have provided is fundamental for understanding the genotypes of populations that evolve by recombination but without mutation. In the case of populations that evolve with mutation, but without recombination, a complementary analysis of fitness landscapes in terms of linear extensions of the genotype (viewed as a poset) is provided by Weinreich (2005). An understanding of the relationship between these approaches will lead to a deeper understanding of populations that evolve by recombination and mutation.

What our study and Weinreich's have in common is that they fall into the domain of non-parametric statistics. In contrast to other papers on fitness landscapes, including (Karlin and Feldman, 1970) and (Kondrashov and Kondrashov, 2001), we do not make *a priori* assumptions about the fitness landscape. In particular, our analysis of the data in Sections 6 and 7 is not based on any choice of model for w . On the other hand, the geometry of the secondary polytope interfaces well with Bayesian statistics, because any family of distributions on $\mathbb{R}^{\mathcal{G}}$ induces a family of distributions on the finite set of possible shapes.

Acknowledgments

This paper was inspired by the DARPA workshop on Fitness Landscapes held at Berkeley in February 2006. We thank Sebastian Bonhoeffer, Richard Lenski and Sally Otto for helpful discussions. N.B. was supported by the Deutsche Forschungsgemeinschaft (BE 3217/1-1). L.P. and B.S. were supported by the DARPA program "Fundamental Laws in Biology" (HR0011-05-1-0057).

References

- Bateson, W. (1909). *Mendel's Principles of Heredity*. Cambridge University Press, Cambridge, UK.
- Beerenwinkel, N., Eriksson, N. and Sturmfels, B. (2006). Evolution on distributive lattices. *J. Theor. Biol.*, to appear.

- Bonhoeffer, S., Chappey, C., Parkin, N. T., Whitcomb, J. M. and Petropoulos, C. J. (2004). Evidence for positive epistasis in HIV-1. *Science* **306(5701)**, 1547–1550.
- Cordell, H. J. (2002). Epistasis: what it means, what it doesn't mean, and statistical methods to detect it in humans. *Hum. Mol. Genet.* **11(20)**, 2463–2468.
- De Loera, J., Rambau, J. and Santos, F. (2006). *Triangulations: Applications, Structures, and Algorithms*. Springer, to appear.
- Feldman, M. W., Franklin, I. and Thomson, G. J. (1974). Selection in complex genetic systems. I. The symmetric equilibria of the three-locus symmetric viability model. *Genetics* **76(1)**, 135–162.
- Fisher, R. A. (1918). The correlations between relatives on the supposition of Mendelian inheritance. *Trans. R. Soc. Edinburgh* **52**, 399–433.
- Gavrilets, S. (2004). *Fitness Landscapes and the Origin of Species*. Princeton University Press.
- Gawrilow, E. and Joswig, M. (2001). Polymake: an approach to modular software design in computational geometry. *Proc. 17th ACM Symposium on Computational Geometry*, Medford, MA.
- Grayson, D. R. and Stillman, M. E. (1999). Macaulay 2, a software system for research in algebraic geometry. <http://www.math.uiuc.edu/Macaulay2/>.
- Grier, D., Huggins, P., Sturmfels, B. and Yu, J. (2006). The hyperdeterminant and triangulations of the 4-cube. *submitted*.
- Hallgrímsdóttir, I. B. (2005). Statistical methods for gene mapping in complex diseases. Ph.D. thesis in Statistics, UC Berkeley.
- Hendy, M. D. and Charleston, M.A. (1993). Hadamard conjugation: a versatile tool for modelling nucleotide sequence evolution. *New Zealand J. Botany* **31**, 231–237.
- Karlin, S. and Feldman, M. W. (1970). Linkage and selection: two locus symmetric viability model. *Theor. Popul. Biol.* **1(1)**, 39–71.
- Kondrashov, F. A. and Kondrashov, A. S. (2001). Multidimensional epistasis and the disadvantage of sex. *Proc. Natl. Acad. Sci. U.S.A.* **98(21)**,

12089–12092.

Lindman, H. R. (1974). *Analysis of Variance in Complex Experimental Designs*. Freeman and Co., San Francisco, CA.

Phillips, P. C. (1998). The language of gene interaction. *Genetics* **149**(3), 1167–1171.

Rambau, J. (2002). TOPCOM: Triangulations of point configurations and oriented matroids. *Proc. Int. Congress of Mathematical Software ICMS*.

Sanjuán, R., Moya, A. and Elena, S. F. (2004). The contribution of epistasis to the architecture of fitness in an RNA virus. *Proc. Natl. Acad. Sci. U.S.A.* **101**(43), 15376–15379.

Segal, M. R., Barbour, J. D. and Grant, R. M. (2004). Relating HIV-1 sequence variation to replication capacity via trees and forests. *Stat. Appl. Genet. Mol. Biol.* **3**(1), 2.

The International HapMap Consortium. (2005). A haplotype map of the human genome. *Nature* **437**(7063), 1299–1320.

Wainberg, M. A. (2004). The impact of the M184V substitution on drug resistance and viral fitness. *Expert Rev. Anti. Infect. Ther.* **2**(1), 147–151.

Weinreich, D. M. (2005). The rank ordering of genotypic fitness values predicts genetic constraint on natural selection on landscapes lacking sign epistasis. *Genetics* **171**(3), 1397–1405.

Whitlock, M. C. and Bourguet, D. (2001). Factors affecting the genetic load in *Drosophila*: synergistic epistasis and correlations among fitness components. *Evolution Int. J. Org. Evolution* **54**(5), 1654–1660.

Wright, S. (1931). Evolution in Mendelian populations. *Genetics* **16**, 97–159.

Ziegler, G. (1995). *Lectures on Polytopes*. Springer, New York, NY.

Department of Mathematics, University of California, Berkeley, CA 94720

E-mail: {niko, lpachter, bernd}@math.berkeley.edu